PHYSICAL REVIEW B VOLUME 11, NUMBER 10 15 MAY 1975

Resonant Raman scattering in silicon

J. B. Renucci,* R. N. Tyte,† and M. Cardona
Max-Planck-Institut für Festkörperforschung, Stuttgart, Federal Republic of Germany

(Received 9 September 1974)

The resonance of the Raman scattering from the zone-center optical phonon in silicon has been measured over a wide energy range covering the 3.4-eV direct band gap. The experimental results are compared with both a theory deriving the Raman cross section from the optical constants and an *ab initio* calculation; good agreement is found in the region where the respective theories are expected to be reliable. The second-order Raman spectrum of silicon has also been measured at laser frequencies between 1.65 and 3.72 eV. Above the 3.4-eV gap, we observe a strong peak in the second-order spectrum corresponding to scattering from two optical phonons near the Γ point. From the resonance behavior of the second-order scattering, several electron–two-phonon deformation potentials are determined.

I. INTRODUCTION

Much attention has been devoted recently to studies of the resonant Raman effect in the diamond and zinc-blende structure semiconductors. In particular, the resonance of both first-order[1] and second-order[2,3] Raman scattering in germanium has been extensively studied in the region of the E_1 and $E_1+\Delta_1$ energy gaps which occur at room temperature at 2.1 and 2.3 eV, respectively. This photon energy region is particularly well suited to studying resonant Raman scattering since it is covered by cw dye lasers and it contains a number of ion laser lines.

Theoretically, the Raman tensor for resonant scattering around E_1 and $E_1+\Delta_1$ is supposed to contain terms due to the modulation of these gaps by the phonons. These terms, called two-band terms, are proportional to the frequency derivative of the dielectric constant and thus should be strongly dispersive near E_1 and $E_1+\Delta_1$. Because of the small splitting $\Delta_1 \simeq 0.2$ eV between the corresponding valence bands there are also so-called three-band contributions which involve the phonon-induced mixing of these valence bands.

Theory and experiment[1] show that in the first-order scattering of germanium the three-band contributions overwhelm the two-band terms in spite of their less strongly resonant character. Consequently, a broad resonance is observed with a maximum between the energies of E_1 and $E_1+\Delta_1$. More recently,[2,3] the resonances of the second-order scattering of germanium have been studied in the same photon energy region. While the first-order scattering has only a $\Gamma_{25'}$ component (the symmetry of the optical phonon at $\vec{k}=0$), Γ_1, $\Gamma_{25'}$, and Γ_{12} components are allowed for the second-order processes. Experiments,[4] however, show that the Γ_{12} component is nearly negligible while the Γ_1 component is dominant. Resonances in the second-order components Γ_1 and $\Gamma_{25'}$ have been observed.[3] As in the first-order scattering the $\Gamma_{25'}$ resonances are due predominantly to three-band terms with the electron–two-phonon interaction playing the role of the electron–one-phonon coupling of the first-order spectrum. These three-band terms are forbidden for the Γ_1 component. Sharp resonances, peaking near E_1 and $E_1+\Delta_1$, are seen for the Γ_1 components. The Γ_1 resonances of features due to peaks in the combined density of two-phonon states can be interpreted as two-band terms with the gap modulation produced by the electron–two-phonon interaction. An even sharper resonance is seen for a Raman peak which occurs at the frequency of two optical phonons of $\vec{k}=0$ (2Γ). This peak is absent for laser energies below 2 eV and can be interpreted as due to the electron–one-phonon interaction acting iteratively in second order.

The phonon spectrum of silicon is essentially the same as that of germanium after scaling the frequencies by the square root of the mass ratio.[5] Consequently, the second-order Raman spectra are also very similar.[6,7] As in germanium the 2Γ peak does not occur below the lowest direct gap, which, however, now takes place around 3.37 eV[8] and corresponds to transitions at Γ between the $\Gamma_{25'}$ valence band and the lowest Γ_{15} conduction band. The band structures of germanium and silicon are thus considerably different. Instead of the $\Gamma_{25'}\rightarrow L_1$ indirect edge of germanium, silicon has a $\Gamma_{25'}\rightarrow\Delta_1$ edge at 1.17 eV (at 1.8 K)[9] (see Fig. 1). The lowest direct edge ($\Gamma_{25'}\rightarrow\Gamma_{15}$ labeled E_0') occurs at 3.37 eV at 77 K and is nearly degenerate with a strong edge at 3.45 eV.[8] Calculations of Kane[11] indicate that this edge is due to transitions along ⟨111⟩ (Λ) (E_1) and also along ⟨100⟩ (Δ) with some contributions from the ⟨110⟩ (Σ) directions. Measurements of wavelength modulated reflectivity under uniaxial stress[12] suggest that the main contribution to the 3.45-eV peak is from ⟨111⟩ (Λ) transitions and is thus analogous to the E_1 edge of germanium. In contrast to germanium, however, the spin-orbit

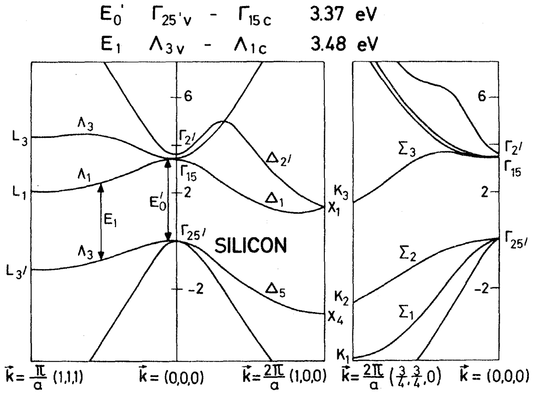

FIG. 1. Band structure of silicon showing the E_0' and E_1 gaps, from Ref. 10.

splitting of this edge (~0.03 eV) is smaller than the lifetime broadening of the transitions and cannot be resolved. Under these conditions it can be shown that the three-band terms in the Raman tensor have essentially the same shape as the two-band contributions: both are proportional to the derivative of the dielectric constant with respect to frequency.

Because of these similarities and differences, and the important role played by silicon among the tetrahedral semiconductors, we have performed first- and second-order resonant Raman scattering experiments in silicon. We have been able to cover the photon energy region between 1.65 and 3.81 eV. The first-order experiments were performed with a pulsed dye laser (2.57–3.41 eV) and with several discrete lines of the He-Cd, Ar$^+$, and Kr$^+$ lasers, including six uv lines up to 3.81 eV. The second-order experiments were performed only with the gas lasers since the scattered intensity, two orders of magnitude lower than for first order, is too small for working with the pulsed dye laser. We were able to show, however, that the shape of the second-order resonance is essentially the same as that of the first-order one and is reasonably well described by $|d\epsilon/d\omega|^2$. From the ratio of the second-order scattered intensities to the first-order ones and the first-order deformation potentials calculated with the pseudopotential method, we were able to obtain the deformation potential for the Γ_1 electron–two-phonon interaction for both optical and acoustic phonons.[13–15] The equivalent of the 2Γ peak observed for germanium near and above E_1 also appears in silicon above 3.4 eV (E_1).

II. THEORY

As indicated in the introduction, the theory we have used to interpret our experimental results is mainly that developed for the earlier work on Ge.[3] Here we will only discuss the main outlines and assumptions and reproduce the necessary results.

The dielectric or quasistatic theory of Raman scattering assumes that the phonon frequency Ω is small compared to the difference between the complex frequency of the appropriate electronic energy gap and that of the laser light, i.e.,

$$\Omega \ll |\omega - \omega_0 + i\eta| ,$$

where ω is the laser frequency, ω_0 the frequency of the energy gap, and η its lifetime broadening. In silicon Ω is larger than in germanium (64 vs 37 meV). However, structure in the optical constants of silicon in the region of direct transitions is nowhere sharper than 0.1 eV.[16] Hence, we are justified in using the quasistatic theory. Under these conditions, the intensity polarized along $\hat{e}_s$ scattered by a field $\vec{\mathrm{E}}$ is given, in terms of the susceptibility tensor $\overleftrightarrow{\chi}$, by

$$I \propto \omega^4 \left| \hat{e}_s \cdot \overleftrightarrow{\mathrm{R}} \cdot \vec{\mathrm{E}} \right| = \omega^4 \left| \hat{e}_{s,j} \frac{d\chi_{jk}}{d\xi_l} E_k \right|^2 \langle \xi_l^2 \rangle , \qquad (1)$$

where ξ_l is the phonon amplitude. For an optical phonon at $\vec{k}=0$ ($\Gamma_{25'}$ symmetry) $d\chi_{jk}/d\xi_l$, and thus the Raman tensor $\overleftrightarrow{\mathrm{R}}$, has only one independent component, which is labeled d_1 in the notation of Loudon.[17] For the E_1 gap there are, as already mentioned in the introduction, two contributions to d_1, one due to the splitting of the equivalent ⟨111⟩ directions by the phonon, determined by the deformation potential $d_{1,0}^5$, and the other determined by $d_{3,0}^5$, a result of the coupling by the phonon of the spin-orbit-split valence Λ_3 bands.[3] The component d_1 of the first-order Raman tensor is thus given by[3]

$$d_1 = \left(\frac{2\sqrt{2}}{\sqrt{3}} \frac{\chi^+ - \chi^-}{\Delta_1} d_{3,0}^5 + \frac{1}{2\sqrt{3}} \frac{d\chi}{d\omega} d_{1,0}^5 \right) \frac{\langle \xi^2 \rangle^{1/2}}{a} , \qquad (2)$$

where χ^+ and χ^-, which determine the three-band terms, are the contributions of the two gaps, E_1 and $E_1 + \Delta_1$, to the scalar susceptibility χ and a is the lattice constant. With a negligible spin-orbit splitting Δ_1, as is the case for silicon, the Λ_3 bands are not coupled but *split* by the phonon (Δ_1 is negligible if it is small with respect to the width η). Under this condition, the three-band terms become two-band terms and only strongly dispersive two-band terms are present. This can be easily seen by taking the limit $\Delta_1 \to 0$ in Eq. (2). We find

$$d_1 = \sqrt{\tfrac{2}{3}} \left(d_{3,0}^5 + \frac{1}{2\sqrt{2}} d_{1,0}^5 \right) \frac{d\chi}{d\omega} \frac{\langle \xi^2 \rangle^{1/2}}{a} . \qquad (3)$$

While $d_{3,0}^5$ refers only to the valence bands, $d_{1,0}^5 = d_{1,0}^5(\mathrm{cond}) - d_{1,0}^5(\mathrm{val})$ has two components due to the conduction (cond) and the valence (val) bands, respectively. Near Γ one can show that $d_{3,0}^5 \simeq -\sqrt{2}\, d_{1,0}^5(\mathrm{val}) \simeq +\sqrt{2}\, d_{1,0}^5$. While moving away from Γ along Λ the ratio $d_{3,0}^5/d_{1,0}^5$ increases in germanium so that on the average for the whole Λ direction the scattering is predominantly determined by $d_{3,0}^5$. The same is true for silicon as shown in Fig. 2. The calculations of Fig. 2 were performed by the pseu-

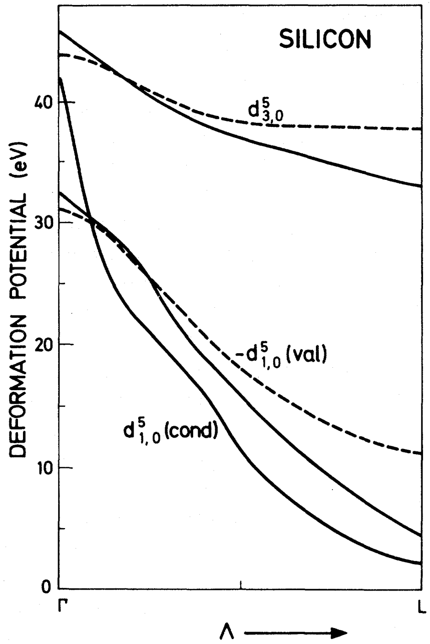

FIG. 2. Deformation potentials $d^5_{1,0}$(cond), $d^5_{1,0}$(val) and $d^5_{3,0}$ of silicon along the Λ direction, as calculated by the $\vec{k}\cdot\vec{p}$ pseudopotential method (solid line, see Appendix) and by the pure pseudopotential method (Ref. 18) (dashed line).

dopotential $-\vec{k}\circ\vec{p}$ method as discussed in the Appendix. Pure pseudopotential calculations, performed by Zeyher,[18] are also shown in Fig. 2. Both sets of calculations disagree with the results obtained from the work of Goroff and Kleinman[19] at the L point (these authors find $d^5_{3,0}=15.4$ eV instead of 37 eV, $d^5_{1,0}(\text{val}) = -3.8$ eV instead of -11 eV, and $d^5_{1,0}(\text{cond}) = +2$ eV instead of -5.2 eV; the values of Goroff and Kleinman and ours, respectively). We do not know the reason for this discrepancy but in view of the reasonable agreement between the two calculations of Fig. 2 we tend to believe our values. As mentioned earlier, there is some contribution of $\langle 100\rangle$ transitions to the 3.4-eV E_1 peak in the optical constants of silicon. This contribution is believed to be small.[12] We nevertheless give the expression for the contribution of these transitions to the first-order resonance Raman tensor $d_1^{\langle 100\rangle}$:

$$d_1^{\langle 100\rangle} = \frac{1}{2}\left(\frac{d\chi}{d\omega}\right)^{\langle 100\rangle} d^t_{4,0}\frac{\langle\xi^2\rangle^{1/2}}{a}\,, \tag{4}$$

where the superscript $\langle 100\rangle$ represents the corresponding contributions and the deformation potential $d^t_{4,0}$ has been defined in Ref. 11. We show in Fig. 3 the values of $d^t_{4,0}$ along Δ calculated with the $\vec{k}\cdot\vec{p}$ pseudopotential method as shown in the Appendix. The average value of $d^t_{4,0}$ near $k=0$ is such that if there is some contribution of Δ transitions to χ the corresponding contribution to d_1 would be somewhat smaller but close to what one would find for $\langle 111\rangle$ transitions of the same strength [Eq. (3)].

As discussed in Refs. 3 and 15 there are two basically different contributions to the resonant second-order spectra. One of them involves the electron-phonon interaction used iteratively twice with resonant final and intermediate states. These terms are more strongly resonant than the first order Raman scattering just discussed but they are only important for phonons with $\vec{k}\approx 0$. The other contributions involve the direct electron–two-phonon interaction,[14,15] renormalized so as to include iterated electron–one-phonon terms with nonresonant energy denominators. These terms have the same resonant shape as the first-order Raman scattering. Their $\Gamma_{25'}$ component near E_1 is described in silicon by Eqs. (3) and (4) with $d^5_{1,0}$, $d^5_{3,0}$, and $d^t_{4,0}$ replaced by the corresponding electron–two-phonon deformation potentials $2\sqrt{2}D^5_1$, $2\sqrt{2}D^5_3$, and $2\sqrt{2}D^t_4$, and $\langle\xi^2\rangle^{1/2}/a$ replaced by $\langle\xi_1^2\rangle^{1/2}\langle\xi_2^2\rangle^{1/2}/a^2$ where the subscripts 1 and 2 label the two phonons involved. For the two-phonon scattering the dominant component is that of Γ_1 symmetry. The resonance near E_1 is represented by the a_2 tensor component (Loudon's notation)[3]

$$a_2 = \frac{4}{3}\frac{d\chi}{d\omega}D_1\frac{\langle\xi_1^2\rangle^{1/2}\langle\xi_2^2\rangle^{1/2}}{a^2}\,, \tag{5}$$

where D_1 is the electron–two-phonon deformation

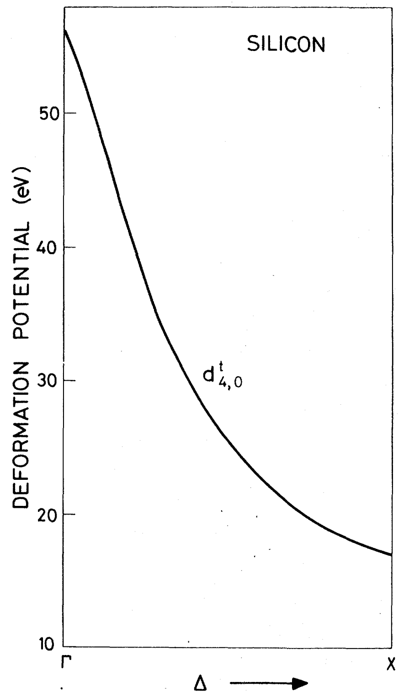

FIG. 3. Deformation potential $d^t_{4,0}$ of the valence bands of silicon along the Δ direction, calculated with the $\vec{k}\cdot\vec{p}$ pseudopotential method (see Appendix).

potential of symmetry Γ_1.

The theory of resonant Raman scattering given above uses the experimentally determined optical constants to predict the spectral dispersion of the Raman cross section. A calculation has been made by Swanson and Maradudin[20] for diamond, silicon, and germanium, which predicts this spectral dependence directly. These authors made a pseudopotential calculation to obtain the electronic susceptibility for a diamond structure lattice distorted in a mode corresponding to a $\vec{k}=0$ optical phonon. The first derivative of the polarizability, the square of which is proportional to the intensity of the Raman scattering, can then be given by

$$P=\lim_{\delta\to 0}\frac{a^2}{\delta}\chi_{xy}\ , \tag{6}$$

where δ represents the magnitude of the sublattice displacement. Values are presented for the coefficients of ω in a Taylor-series expansion of P about $\omega=0$, that is, $P^{(n)}$ in

$$P=P^{(0)}+P^{(1)}\omega^2+P^{(2)}\omega^4+P^{(3)}\omega^6 \tag{7}$$

for different values of δ.

This calculation is expected to be valid at energies well below the first direct band gap; not only is the Taylor expansion itself about $\omega=0$ but the calculation of the electronic susceptibility ignores imaginary contributions, which have a significant effect on the Raman tensor in the region of direct transitions.

Of the three materials for which calculations were presented, it is thus clear that silicon is the best suited for experimental investigation; in germanium, the first direct gap is sufficiently low in energy ($E_0=0.79$ eV) to prevent resonant Raman measurements below E_0, and in diamond the gap is so large that no significant dispersion in the visible region is anticipated. In silicon, however, the 3.4-eV direct gap lies towards the high-energy end of available laser sources; measurements can conveniently be made down to energies less than one-half of the direct band gap.

III. EXPERIMENTS

The Raman experiments reported here were made in the back scattering mode on a single crystal of Si. The laser light was scattered from a (100) face which had been mechanically polished, etched in CP4, and polished with Syton X30 (Monsanto Corp.). This final polishing has proved essential for a good rejection of scattering of fluorescent light from the dye laser which otherwise obscures the Raman signal.[21] The incoming light was in all experiments polarized parallel to [010] and no analyzer was used. Under these conditions, the first order scattering is allowed only in the parallel/perpendicular configuration, i.e., the allowed scattering geometry was $Z(X,Y)\bar{Z}$; in second order the $\Gamma_1+4\Gamma_{12}$ symmetry components are scattered in the parallel/parallel configuration and the $\Gamma_{25'}$ component in the parallel/perpendicular one. Because of the time-consuming second-order measurements, we did not attempt to separate the Γ_1 and $\Gamma_{25'}$ components. These components have been separated at[6] 514.5 and at[7] 488 nm; since their ratio is the same at these two wavelengths we extracted the Γ_1 and $\Gamma_{25'}$ components from our measurements by assuming that their ratio is independent of scattering wavelength and using the results of Refs. 6 and 7. The ratio of the throughputs of the spectrometer for the horizontal and vertical polarizations was also taken into account.

The experimental system, using a nitrogen laser pumped pulsed dye laser, has been described in detail elsewhere[21]; here it suffices to point out that the laser is continuously tunable from the red-yellow region (575 nm) to 360 nm in the ultraviolet using a variety of dyes. Table I lists the dye and solvent combinations we employed in our experiments. The mean power obtained is relatively low, of the order of 3 mW in the blue, being reduced to 300 μW in the ultraviolet. A gate is used in the photon counting system, which is synchronized to the firing of the nitrogen pump laser; this reduces the observed dark counts of the system by a factor 2×10^3 at 100 pulses/sec and permits Raman sig-

TABLE I. Dyes, solvents, concentrations, and tuning ranges obtained.

Dye	Solvent	Concentration	Tuning range (nm)
7-diethylamino-4-methylcoumarin	Methanol	5×10^{-3} *M*	483–443
7-ethylamino-4, 6-dimethylcoumarin	Methanol	5×10^{-3} *M*	473–435
7-amino-4-methyl-coumarin	Methanol	5×10^{-3} *M*	459–423
1,4-di-[2-(5-phenoxazolyl)]-benzene	Toluene	1×10^{-3} *M*	423–417
Diphenyl stilbene	Toluene	saturated	414–405
2-(1-naphthyl)-5-phenyloxazole	Toluene	5×10^{-3} *M*	409–398
AVCO 17/67[a]			398–380
AVCO 17/50[a]			379–360

[a] AVCO Everett Research Laboratory.

nals of the order of a few counts/sec to be observed and measured.

In addition to the pulsed dye laser, the cw laser emission from a Spectra Physics 170 argon laser, a Spectra Physics 165 krypton laser and a Spectra Physics 185 helium-cadmium laser were used to extend the first-order data further into the ultraviolet and also into the infrared; with these lasers six lines between 363.8 and 325 nm are obtained. The spectra taken with cw lasers were recorded in a conventional photon counting mode. Great care was used to match points taken with different lasers; uv spectra from the different lasers were compared with spectra obtained in the visible with the same laser and these latter points were compared by overlapping the wavelengths with those of the dye laser. In addition, the highest-energy dye laser point taken was in coincidence with the 363.8-nm argon-ion line, thus providing a check on the accuracy of the comparison.

The heights of the Raman peaks measured with the pulsed dye laser were corrected for the saturation effect which can be observed at counting rates not small compared to the repetition rate of the laser; the true counting rate is given by[21]

$$R = -\ln(1 - R_{\text{obs}}) ,$$

where R_{obs} is the observed counting rate.

The second-order scattering in Si is two orders of magnitude weaker than the first order and it proved not possible to measure this using the pulsed dye laser; spectra were therefore only taken with cw laser lines.

IV. RESULTS AND DISCUSSION

A. First-order scattering

Figure 4 shows our results for the resonance of the first-order phonon scattering in Si between 2.35 and 3.81 eV. The data were compared to CaF_2, as is usual for resonant Raman scattering measurements, in order to provide a calibration for the spectral response of the entire apparatus; the ω^4 dependence of the scattering cross section is also automatically removed by this procedure. Since the radiating volume is proportional to the absorption coefficient (provided $1/\alpha$ is smaller than the thickness of the sample, a condition which holds for our measurements) we had to correct our data by multiplying them by α. The absorption coefficient was obtained from the transmission measurements of Dash and Newman[22] between 1.1 and 3.4 eV, and from a Kramers-Kronig analysis of reflectivity data by Philipp.[16] Both sets of data agree within their region of overlap. The matching of data points taken with different lasers over the whole curve is seen to be good; the close agreement between the two independent points taken at 3.54 eV (350 nm) (from the argon and krypton ion lasers, each being separately normalized to dye laser points in the blue) is particularly satisfying.

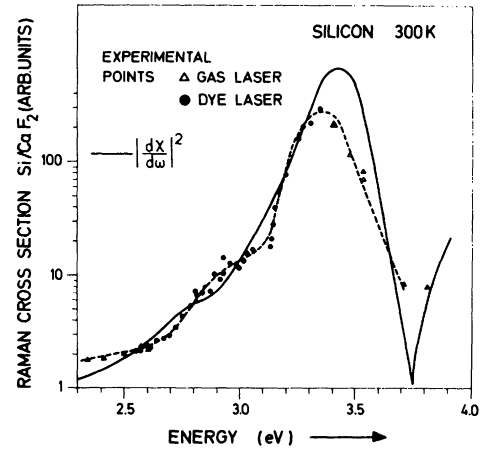

FIG. 4. Raman cross section of first-order phonon in silicon as a function of the photon energy of the laser (points). Also, theoretical dependence $| d_{\chi}/d\omega |^2$ obtained from the data of Ref. 16 (solid line).

The most prominent feature of the experimental results is the peak observed at 3.35 eV; in addition, a shoulder is present on this main peak in the region 2.9–3.0 eV. The former feature clearly corresponds to the expected resonance at the E_0' and E_1 gaps; the latter was not anticipated as there have been no previous reports of structure in the optical constants of Si in this energy region. As a comparison, we show the curve for $| d\chi/d\omega |^2$ obtained from the dielectric constant of Philipp[16] fitted to the experimental data by means of a multiplicative factor. According to Sec. II, this curve should represent the experimental data if only one set of interband transitions is present or, in the case of several sets (above 3.7 eV one sees the beginning of the E_2 transitions), if the various deformation potentials involved are equal. The agreement between this theoretical curve and experiment is as good as expected considering the possible errors involved in performing the absorption correction with an absorption coefficient obtained from a Kramers-Kronig analysis.

The main peak is theoretically predicted at 3.43 eV; the experimental value of 3.35 eV is clearly a little low. However, a shift of the entire theoretical curve to lower energies makes the over-all fit away from the main peak significantly worse. Shifts of the same magnitude *but opposite sign* are often encountered between experimental and theoretical resonant Raman curves.[3] A shift of the experimental curve to lower energies could be due to heating of the sample by the laser radiation. This possibility, however, must be discarded in view of the

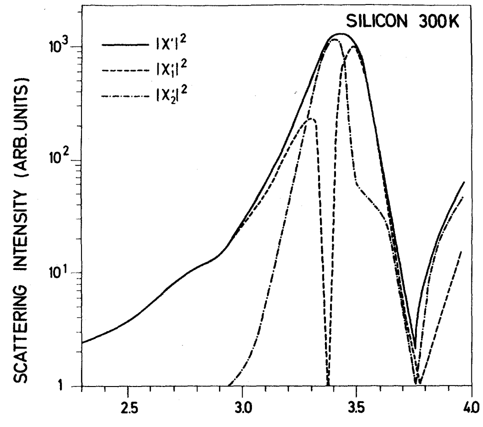

FIG. 5. Separate contribution of the real (χ_1') and the imaginary (χ_2') parts of the first derivative of χ to the theoretical curve of Fig. 4.

observed independence of the shift on average and peak laser power. The shift may be due to inaccuracies in the Kramers-Kronig analyzed coefficient α which was used for the absorption correction. We thus cannot decide whether to attribute any fundamental significance to this shift.

The shoulder observed in the experimental data around 2.9 eV seems to correspond to a somewhat weak shoulder in the theoretical $|d\chi/d\omega|^2$. This shoulder is probably related to the strong increase in the imaginary part of χ in this region and the related effect in χ_1 (see Fig. 5); it is the edge leading to the $E_0' - E_1$ peak, probably due to indirect transitions. The experimental shoulder, somewhat stronger than the calculated one, must represent an enhancement of this edge with respect to the rest of the resonant spectrum due to an increased electron-phonon coupling mechanism. We are not, at present, in a position to make more precise statements about this matter.

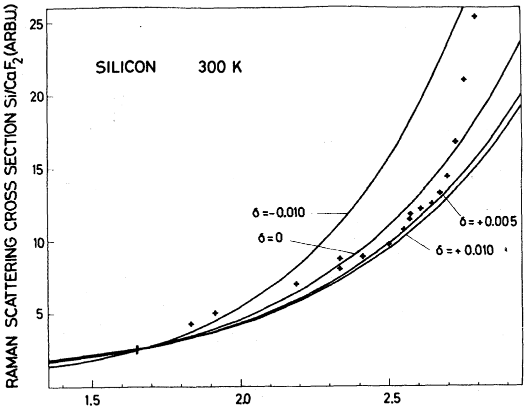

FIG. 6. Raman cross section of first-order phonon in silicon as a function of photon energy of the laser (points) at energies well below the direct band gap. Also, theoretical predictions from Eq. (7) for various values of δ (see text).

TABLE II. Values of $P^{(n)}$ in Eq. (7), used to fit data of Fig. 6; for nonzero δ from Swanson and Maradudin (Ref. 20), for $\delta = 0$ our interpolation.

δ	$P^{(0)}$	$P^{(1)}$	$P^{(2)}$	$P^{(3)}$
+0.010	8.62	1.88	0.25	0.03
+0.005	7.67	1.75	0.24	0.03
0	6.73	1.62	0.23	0.06
−0.010	4.91	1.37	0.20	0.20

In Fig. 6, we give additional experimental data for the low energy tail of the resonance; experimental points are shown, corrected as those of Fig. 4, for photon energies of 1.65–2.80 eV. This energy range, corresponding to 0.42–0.82 E_0', is a suitable one for comparison between experiment and the *ab initio* calculations of Swanson and Maradudin[20] discussed above.

We thus also show in Fig. 6 the theoretical curves for the Raman cross section of Si, derived from Eq. (7), for four values of the parameter δ, the sublattice displacement. These are the three values used by Swanson and Maradudin, together with our interpolated values for $\delta = 0$, using a quadratic expression to fit $P^{(n)}(\delta)$. The values of $P^{(n)}$ are given in Table II. The theoretical curves were fitted to experiment by varying a multiplicative factor so as to bring them into coincidence at the lowest-energy datum point at 1.65 eV. Though somewhat arbitrary, this procedure is justified by remembering that the theory is expected to be most reliable at the lowest photon energies. It is seen that the agreement between theory and experiment in the energy region 1.65–2.70 eV is remarkably good, a best-fit curve lying between those shown for $\delta = 0$ and $\delta = 0.005$. Swanson and Maradudin point out that their values of $P^{(n)}$ are not expected to be reliable to better than 20% and we note that the differences in the $P^{(n)}$ for these two values of δ are all less than this expected error, with the exception of $P^{(3)}$, the highest-order coefficient. Within this energy range, we are thus able to say that the theory reproduces experiment to within an accuracy comparable to the anticipated errors.

Above 2.7 eV, the slope of the experimental curve increases sharply to give the shoulder at around 2.9 eV already commented on; this feature is not shown by the theoretical curves.

B. Second-order scattering

The variation of the shape of the second-order 2TO spectrum[6,7] is shown in Fig. 7. We have in-

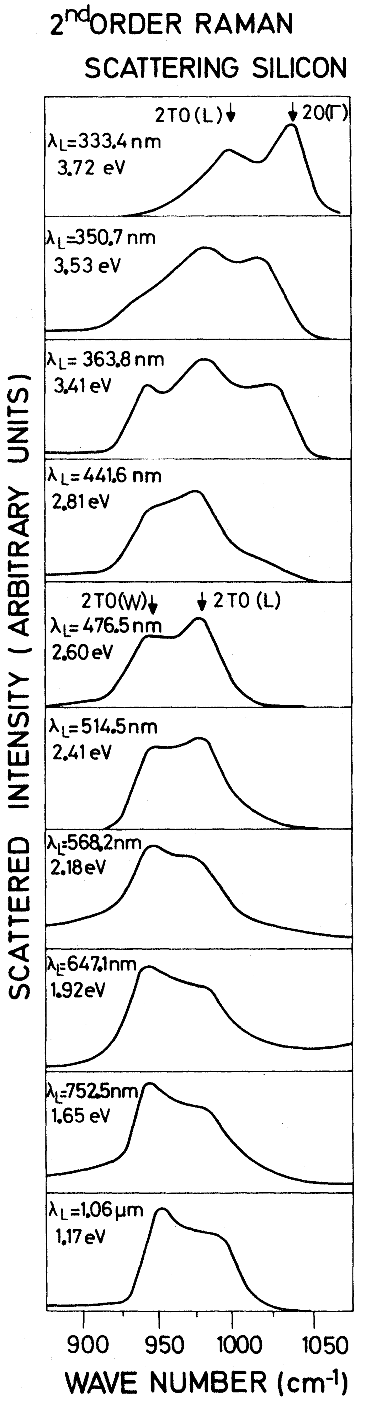

FIG. 7. Second-order 2TO spectra of silicon for ten different laser frequencies. The data at 1.17 eV are from Ref. 23.

cluded in this figure the data of Klein *et al.*[23] obtained with a Nd-YAG laser at 1.17 eV. The spectrum keeps the same shape, very similar to the density of phonon states[5] with the horizontal scale expanded by two, between 2.41 and 2.81 eV. Above 2.81 eV, a shoulder develops at an energy slightly below that which corresponds to two optical phonons at Γ. This peak is similar to that observed for Ge above E_1 and interpreted as due to the iterated first-order electron-phonon interaction with resonant intermediate states.[3] The wave-number of the maximum of this structure depends on laser frequency in agreement with theoretical considerations. Above the gap, for example, the intermediate state is resonant for a phonon momentum which depends on laser frequency. The change in resonant phonon momentum produces a dependence of the scattering peak on laser frequency. In fact, the behavior shown in Fig. 7, a sharpening and a shift closer to the 2TO(Γ) energy with increasing laser frequency is very similar to that of Fig. 12 of Ref. 3. This peak seems to be still sharpening at 3.72 eV, thus suggesting that the most strongly contributing resonant gap is not E_1 but either E_0 (4.1 eV) or E_2 (4.3 eV).[24] We also notice in Fig. 7 that the 2TO(W) peak disappears between 3.54 and 3.72 eV. A similar effect has been observed for germanium: actually, the 3.54-eV spectrum of Fig. 7 looks much like that of germanium at 2.6 eV. This effect was interpreted[3] as an iterated resonance with an intermediate state differing in $\vec{k}$ from that of the initial state by the $\vec{k}$ of the phonons involved. It was thus suggested that the resonance was associated with the indirect gap between the $L_{3'}$ critical point of the valence band and the first maximum in the density of conduction states. From available sources[8,25] we find that this gap amounts to 3.7 eV in silicon and can therefore explain the observed 2TO(L) enhancement over 2TO(W). This explanation must remain tentative until the measurements are extended to higher energies.

The relative heights of the 2TO(W) and 2TO(L) peaks of Fig. 7 reverse between 2.18 and 2.41 eV. This effect has also been explained as an enhancement of scattering from phonons near 2TO(X) (with a $\vec{k}$ equal to that of the indirect gap) due to the 1.1-eV indirect gap.[23] Like most iterated resonances,[3] this effect is expected to increase sharply below the indirect gap and to stay nearly constant a considerable range within the gap, thus accounting for the observed behavior.

The 2TA spectrum, which contains only Γ_1 components,[7] is shown in Fig. 8 at four different photon energies. The enhancement of the 2TA(X) peak at low photon energies has been also attributed[23] to iterated processes with the indirect gap as intermediate state. This enhancement also decays slowly above the indirect gap, in a manner similar to that discussed for the 2TO spectrum.

Figure 9 shows the height of the observed 2TO(W) and 2TO(L) peaks as a function of laser frequency. We have fitted these points with the function $|d\chi/d\omega|^2$ of Fig. 5. The fit is sufficiently good to enable us to use the theory of Sec. II, Eqs. (3) and

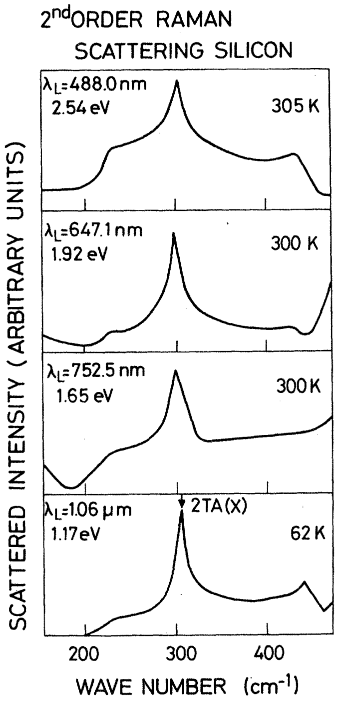

FIG. 8. Second-order 2TA spectra of silicon for four different laser frequencies. The data at 1.17 eV are from Ref. 23. Those at 2.54 eV from Ref. 7.

TABLE III. Deformation potentials calculated with Eqs. (3) and (5) in eV for TO and TA phonons in Si at the E_1 gap. Also shown are the analogous deformation potentials found for the E_1 edge of Ge and the E_0 edges of GaP, ZnTe, and InSb.

			D_3^5, D_{15}		
		D_1	$D_3^5+(1/2\sqrt{2})D_1^5(\mathrm{Si})$	D_1^5	D_3^3
$\mathrm{Si}(E_1)$	2TO	1220	350	⋯	⋯
	2TA	80	⋯	⋯	⋯
Ge (E_1)[a]	2TO	2535	540	0	470
	2TA	170	0	0	0
GaP (E_0)[b]	2TO	1670	⋯	⋯	⋯
	2LO	2180	⋯	⋯	⋯
	TO + LO	⋯	450	⋯	⋯
	2TA	675	⋯	⋯	⋯
ZnTe (E_0)[c]	2TA	575	⋯	⋯	⋯
	2LO	0	⋯	⋯	⋯
	TA + LO	⋯	340	⋯	⋯
	TO + LO	⋯	160	⋯	⋯
InSb (E_0)[d]	2TA	15 000	⋯	⋯	⋯
	2TO	620	⋯	⋯	⋯

[a] From Ref. 3.

[b] From Ref. 26, with numerical corrections as given in Ref. 2.

[c] From Ref. 27.

[d] From Ref. 28.

(5), to obtain from the ratio of the areas under the 2TO [excluding contributions from 2TO(Γ)] and the first-order spectrum the ratio of the corresponding deformation potentials. We note, however, that the measured points lie above the $|d\chi/d\omega|^2$ line at low energies. A better fit could be obtained by adding a constant to $d\chi/d\omega$. The ratio of the areas at 3.41 eV is 0.0833 for the Γ_1 component of the 2TO spectrum, and using the average potentials $d_{3,0}^5 = 38$ eV and $d_{1,0}^5 = 4$ eV of Fig. 3, we find $D_1 = 1220$ eV for the 2TO phonons. From the ratio of Γ_1 and $\Gamma_{25'}$ components of the 2TO scattering, measured by other workers[6,7] to be 4.1 at both 488 and 514.5 nm, we then calculate $D_3^5 + (1/2\sqrt{2})D_1^5 = 350$ eV. From the ratio of the 2TA to the first-order area at 3.41 eV we find $D_1(\mathrm{2TA}) = 80$ eV. These electron–two-phonon deformation potentials are compared in Table III with those obtained for other materials both at the E_1 gap (germanium) and at the E_0 gap (InSb, GaP, ZnTe). Perhaps the most meaningful comparison is that to germanium since the same gap is involved. We find the deformation potentials of both materials to be similar but somewhat smaller for silicon, a reflection of the weaker core potential produced by the smaller nuclear charge.[15] We point out that electron–two-phonon deformation potentials several times higher than those reported here have been obtained from an analysis of mobility data for the Δ_1 conduction band of Si.[29,30]

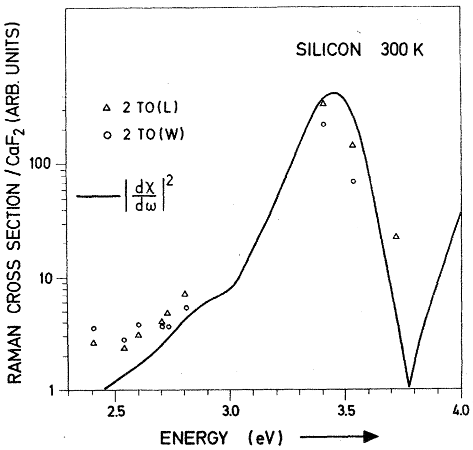

FIG. 9. Raman cross section of second-order 2TO(*W*) and 2TO(*L*) phonons in silicon as a function of the laser energy. Also theoretical dependence $|d\chi/d\omega|^2$ obtained from the data of Ref. 16 (solid line).

ACKNOWLEDGMENTS

We would like to thank S. Go and R. Zeyher for most useful discussions, and H. R. Philipp for providing the numerical data from his Kramers-Kronig analysis.

APPENDIX

The purpose of this Appendix is to determine the electron–one-phonon deformation potentials of the valence and conduction bands in the [111] direction using the pseudopotential $-\vec{k}\cdot\vec{p}$ method.

The eigenvalues and eigenfunctions of the valence and conduction states at $\vec{k}=0$ can be determined in the pseudopotential formalism as a mixture of plane waves of wave vectors $(2\pi/a)(0,0,0)$, $2\pi/a(1,1,1)$ and $2\pi/a(2,0,0)$.[31]

We shall denote these 15 plane waves as follows[32]:

$$w_0=[000],\ w_1=[111],\ w_2=[1\bar{1}\bar{1}],\ w_3=[\bar{1}1\bar{1}],\ w_4=[\bar{1}\bar{1}1],$$
$$w_5=[\bar{1}\bar{1}\bar{1}],\ w_6=[\bar{1}11],\ w_7=[1\bar{1}1],\ w_8=[11\bar{1}],\ W_1=[200], \tag{A1}$$
$$W_2=[020],\ W_3=[002],\ W_4=[\bar{2}00],\ W_5=[0\bar{2}0],\ W_6=[00\bar{2}].$$

The symmetrized combination $[ijk]_\Gamma$ of the waves $[ijk]$ belonging to the Γ representation are given in Ref. 32 and are labeled

$$\begin{gathered}[000]_{\Gamma_1},\\ [111]_{\Gamma_1},\ [111]_{\Gamma_{25'}},\ [111]_{\Gamma_{15}},\ [111]_{\Gamma_{2'}},\\ [200]_{\Gamma_{12'}},\ [200]_{\Gamma_{25'}},\ [200]_{\Gamma_{2'}}\ .\end{gathered} \tag{A2}$$

The pseudopotential removes some of the above degeneracies by coupling states of the same symmetry. The states of symmetry Γ_{15} and Γ_{12} are unchanged whereas those of symmetry Γ_1, $\Gamma_{2'}$, and $\Gamma_{25'}$ are given by diagonalizing 2×2 matrices.[31] Using the form factors given by Brust[33] one gets for the pseudo-eigenvectors:

$$\begin{aligned} |\Gamma_1^l\rangle &= \eta[000]_{\Gamma_1}+\theta[111]_{\Gamma_1}\ , & |\Gamma_1^u\rangle &= -\theta[000]_{\Gamma_1}+\eta[111]_{\Gamma_1}\ ,\\ |\Gamma_{2'}^l\rangle &= \lambda[111]_{\Gamma_{2'}}+\mu[200]_{\Gamma_{2'}}\ , & |\Gamma_{2'}^u\rangle &= -\mu[111]_{\Gamma_{2'}}+\lambda[200]_{\Gamma_{2'}}\ ,\\ |\Gamma_{25'}^l\rangle &= \beta[111]_{\Gamma_{25'}}+\gamma[200]_{\Gamma_{25'}}\ , & |\Gamma_{25'}^u\rangle &= -\gamma[111]_{\Gamma_{25'}}+\beta[200]_{\Gamma_{25'}}\ ,\end{aligned} \tag{A3}$$

where

$$\eta=0.903\ ,\quad \theta=0.430\ ,\quad \lambda=0.816\ ,\quad \mu=0.577\ ,\quad \beta=0.793\ ,\quad \gamma=0.605\ .$$

Because of the symmetry of the $\Gamma_{25'}$ optical phonon which corresponds to a shift of the two sublattices along the [111] direction it is convenient to work in the coordinate system

$$\begin{gathered}\bar{x}=(1/\sqrt{2})(x-y)\ ,\quad \bar{y}=(1/\sqrt{6})(x+y-2z)\ ,\\ \bar{z}=(1/\sqrt{3})(x+y+z)\ ,\end{gathered} \tag{A4}$$

In this system the symmetrized plane waves are

$$\begin{aligned}
&[000]_{\Gamma_1}=w_0\ ,\\
&[111]_{\Gamma_1}=(1/\sqrt{8})(w_1-w_2-w_3-w_4+w_5-w_6-w_7-w_8),\\
&[111]_{\Gamma_{2'}}=(1/\sqrt{8})(w_1-w_2-w_3-w_4-w_5+w_6+w_7+w_8),\\
&[200]_{\Gamma_{2'}}=(1/\sqrt{6})(W_1+W_2+W_3-W_4-W_5-W_6),\\
&[200]_{\Gamma_{12'}^{(2)}}=\tfrac{1}{2}(W_1-W_2-W_4+W_5),\\
&[111]_{\Gamma_{25'}^{\bar{x}}}=\tfrac{1}{2}(-w_2+w_3-w_6+w_7),\\
&[200]_{\Gamma_{25'}^{\bar{x}}}=\tfrac{1}{2}(W_1-W_2+W_4-W_5),\\
&[111]_{\Gamma_{25'}^{\bar{z}}}=(1/\sqrt{24})(3w_1+w_2+w_3+w_4+3w_5+w_6\\
&\qquad +w_7+w_8),\\
&[200]_{\Gamma_{25'}^{\bar{z}}}=(1/\sqrt{6})(W_1+W_2+W_3+W_4+W_5+W_6),\\
&[111]_{\Gamma_{15}^{\bar{x}}}=\tfrac{1}{2}(-w_2+w_3+w_6-w_7),\\
&[111]_{\Gamma_{15}^{\bar{z}}}=(1/\sqrt{24})(3w_1+w_2+w_3+w_4\\
&\qquad -3w_5-w_6-w_7-w_8).
\end{aligned} \tag{A5}$$

Once the states at $\vec{k}=0$ are known, it is possible using the full $\vec{k}\cdot\vec{p}$ representation to get the eigenvalues and eigenvectors at any point of the Brillouin zone.[34] In the [111] direction the states which correspond to one of the components of the doubly degenerate Λ_3^v valence band and to the nondegenerate Λ_1^c conduction band are

$$\begin{aligned}
|\psi_3^v\rangle_{111} &= A\,|\Gamma_{25'}^l(\bar{X})\rangle+B\,|\Gamma_{15}(\bar{x})\rangle+C\,|\Gamma_{25'}^u(\bar{X})\rangle+D\,|\Gamma_{12'}^{(2)}\rangle,\\
|\psi_1^c\rangle_{111} &= A'\,|\Gamma_{2'}^l\rangle+B'\,|\Gamma_{2'}^u\rangle+C'\,|\Gamma_1^l\rangle+D'\,|\Gamma_1^u\rangle\\
&\quad +E'\,|\Gamma_{25'}^l(\bar{Z})\rangle+F'\,|\Gamma_{25'}^u(\bar{Z})\rangle+G'\,|\Gamma_{15}(\bar{z})\rangle\ .
\end{aligned} \tag{A6}$$

The coefficients $A, B, \ldots, A', B', \ldots,$ are given in Ref. 34.

Let us compute now the effect of a $\Gamma_{25'}$ optical phonon on the Λ_3^v valence band and the Λ_1^c conduction band.

1. Λ_3^v valence band

The effect of a $\Gamma_{25'}$ phonon, is similar to that of a uniaxial stress along the [111] direction, as shown in Fig. 10:

(i) the equivalent ⟨111⟩ directions are split; this effect is represented by the deformation potential $d_{1,0}^5$.

(ii) the spin-orbit-split valence bands are coupled; this is represented by the deformation

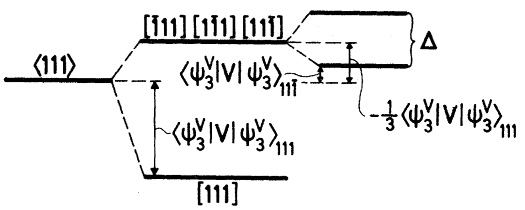

FIG. 10. Splitting pattern of the valence bands of silicon along the ⟨111⟩ direction.

potential $d^5_{3,0}$.

If one assumes that the atomic form factor is not affected by the $\Gamma_{25'}$ phonon only the structure factor changes: $2\vec{\tau}$, the distance between the two atoms in the primitive cell, becomes $2\vec{\tau}\,' = \frac{1}{4}a(1+\delta, 1+\delta, 1+\delta)$ where δ represents the magnitude of the sublattice displacement. The energies are then modified by the perturbating potential $V=\sum_{|q|\leq 12} - v_q \vec{q}\cdot\vec{\tau}\delta \sin\vec{q}\circ\vec{\tau}$ ($\vec{q}$ is a reciprocal-lattice vector). First-order perturbation theory enables us to calculate the perturbed energies by calculating the matrix elements: $\langle\psi^v_3|V|\psi^v_3\rangle_{111}$ and $\langle\psi^v_3|V|\psi^v_3\rangle_{11\bar{1}}$. Using the expressions (A3, A5, A6) and taking into account the symmetry one finds

$$\langle\psi^v_3|V|\psi^v_3\rangle_{111} = (A\beta - C\gamma)^2\langle[111]_{\Gamma^{\bar{X}}_{25'}}|V|[111]_{\Gamma^{\bar{X}}_{25'}}\rangle + B^2\langle[111]_{\Gamma^{\bar{x}}_{15}}|V|[111]_{\Gamma^{\bar{x}}_{15}}\rangle$$
$$+[2\beta\gamma(A^2-C^2)+2AC(\beta^2-\gamma^2)]\langle[111]_{\Gamma^{\bar{X}}_{25'}}|V|[200]_{\Gamma^{\bar{X}}_{25'}}\rangle + 2BD\langle[111]_{\Gamma^{\bar{x}}_{15}}|V|[200]_{\Gamma^{(2)}_{12'}}\rangle\ , \qquad \text{(A7)}$$

where

$$\langle[111]_{\Gamma^{\bar{X}}_{25'}}|V|[111]_{\Gamma^{\bar{X}}_{25'}}\rangle = (v_4 - v_{12})(\pi/2)\delta \qquad \langle[111]_{\Gamma^{\bar{X}}_{25'}}|V|[200]_{\Gamma^{\bar{X}}_{25'}}\rangle = (v_3 - v_{11})(\pi\sqrt{2}/4)\delta\ ,$$
$$\langle[111]_{\Gamma^{\bar{x}}_{15}}|V|[111]_{\Gamma^{\bar{x}}_{15}}\rangle = (v_{12} - v_4)(\pi/2)\delta\ , \qquad \langle[111]_{\Gamma^{\bar{x}}_{15}}|V|[200]_{\Gamma^{(2)}_{12'}}\rangle = (v_3 - v_{11})(\pi\sqrt{2}/2)\delta\ . \qquad \text{(A8)}$$

One calculates in the same way $\langle\psi^v_3|V|\psi^v_3\rangle_{11\bar{1}}$, noting that

$$|\psi^v_3\rangle_{11\bar{1}} = -A|\Gamma^l_{25'}(\bar{X})\rangle + B|\Gamma_{15}(\bar{x})\rangle - C|\Gamma_{25'}(\bar{X})\rangle - D|\Gamma^{(2)}_{12'}\rangle\ .$$

The definitions of the deformation potentials for a uniaxial stress along a [111] direction[35] give, for a $\Gamma_{25'}$ phonon,[31]

$$d^5_{1,0}(\text{val}) = (8/\sqrt{3})(1/\delta)\langle\psi^v_3|V|\psi^v_3\rangle_{111}$$

and

$$d^5_{3,0} = (2\sqrt{3}/\sqrt{2})(\Delta/\delta)\ , \qquad \text{(A9)}$$

where

$$\Delta = 2[-\langle\psi^v_3|V|\psi^v_3\rangle_{11\bar{1}} - \tfrac{1}{3}\langle\psi^v_3|V|\psi^v_3\rangle_{111}]\ .$$

Using the form factors of Ref. 33 and the values of $A, B, \ldots,$ given in Ref. 34, Eqs. (A9) yield $d^5_{1,0}$(val) and $d^5_{3,0}$ along the [111] direction. The results are shown in Fig. 2.

2. Λ^c_1 conduction band

In the Λ^c_1 conduction-band case the $\Gamma_{25'}$ phonon splits only the equivalent ⟨111⟩ directions and one finds

$$d^5_{1,0}(\text{cond}) = (8/\sqrt{3})(1/\delta)\langle\psi^c_1|V|\psi^c_1\rangle_{111}\ , \qquad \text{(A10)}$$

with

$$\langle\psi^c_1|V|\psi^c_1\rangle = (E'\beta - F'\gamma)^2\langle[111]_{\Gamma^{\bar{z}}_{25'}}|V|[111]_{\Gamma^{\bar{z}}_{25'}}\rangle + [2\beta\gamma(E'^2 - F'^2) + 2E'F'(\beta^2-\gamma^2)]$$
$$\times\langle[111]_{\Gamma^{\bar{z}}_{25'}}|V|[200]_{\Gamma^{\bar{z}}_{25'}}\rangle + G'^2\langle[111]_{\Gamma^{\bar{z}}_{15}}|V|[111]_{\Gamma^{\bar{z}}_{15}}\rangle + 2G'(\lambda A' - \mu B')\langle[111]_{\Gamma_{2'}}|V|[111]_{\Gamma^{\bar{z}}_{15}}\rangle$$
$$+2G'(\mu A' + \lambda B')\langle[200]_{\Gamma_{2'}}|V|\Gamma^{\bar{z}}_{15}\rangle + 2(C'E'\eta\beta - C'F'\eta\gamma - D'E'\theta\beta + D'F'\theta\gamma)\langle[000]_{\Gamma_1}|V|[111]_{\Gamma^{\bar{z}}_{25'}}\rangle$$
$$+2(C'E'\eta\gamma + C'F'\eta\beta - D'E'\theta\gamma - D'F'\theta\beta)\langle[000]_{\Gamma_1}|V|[200]_{\Gamma^{\bar{z}}_{25'}}\rangle$$
$$+2(C'E'\theta\beta - C'F'\theta\gamma + D'E'\eta\beta - D'F'\eta\gamma)\langle[111]_{\Gamma_1}|V|[111]_{\Gamma^{\bar{z}}_{25'}}\rangle$$
$$+2(C'E'\theta\gamma + C'F'\theta\beta + D'E'\eta\gamma + D'F'\eta\beta)\langle[111]_{\Gamma_1}|V|[200]_{\Gamma^{\bar{z}}_{25'}}\rangle\ . \qquad \text{(A11)}$$

where

$$\langle[111]_{\Gamma^{\bar{z}}_{25'}}|V|[111]_{\Gamma^{\bar{z}}_{25'}}\rangle = (v_{12} - v_4)\pi\delta\ , \quad \langle[111]_{\Gamma^{\bar{z}}_{25'}}|V|[200]_{\Gamma^{\bar{z}}_{25'}}\rangle = (v_{11} - v_3)(\pi\sqrt{2}/2)\delta\ ,$$
$$\langle[111]_{\Gamma^{\bar{z}}_{15}}|V|[111]_{\Gamma^{\bar{z}}_{15}}\rangle = (v_4 - v_{12})\pi\delta\ , \quad \langle[111]_{\Gamma_{2'}}|V|[111]_{\Gamma^{\bar{z}}_{15}}\rangle = -(v_4 + v_{12})(\pi\sqrt{3}/2)\delta\ ,$$
$$\langle[200]_{\Gamma_{2'}}|V|[111]_{\Gamma^{\bar{z}}_{15}}\rangle = -(v_3 + 5v_{11})(\pi\sqrt{2}/4)\delta\ , \quad \langle[000]_{\Gamma_1}|V|[111]_{\Gamma^{\bar{z}}_{25'}}\rangle = -v_3(\pi\sqrt{3}/2)\delta\ , \qquad \text{(A12)}$$
$$\langle[000]_{\Gamma_1}|V|[200]_{\Gamma^{\bar{z}}_{25'}}\rangle = -v_4\pi\sqrt{\tfrac{3}{2}}\delta\ , \quad \langle[111]_{\Gamma_1}|V|[111]_{\Gamma^{\bar{z}}_{25'}}\rangle = (v_4 + v_{12})(\pi\sqrt{3}/2)\delta\ ,$$
$$\langle[111]_{\Gamma_1}|V|[200]_{\Gamma^{\bar{z}}_{25'}}\rangle = (v_3 + 3v_{11})(\pi\sqrt{6}/4)\delta\ ,$$

The curve of Fig. 2 was obtained using Eqs. (A10)–(A12). One can also calculate the deformation potential $d^t_{4,0}$ along the [100] direction. Using the definition of Kane[35] one gets $d^t_{4,0} = (8/\delta)\langle\psi|V|\psi\rangle_{100}$, where

$$|\psi\rangle_{100} = A''\,|\Gamma^{l}_{25'}(\bar{X})\rangle + B''\,|\Gamma_{15}(\bar{x})\rangle + C''\,|\Gamma^{u}_{25'}(\bar{X})\rangle \tag{A13}$$

and

$$\begin{aligned}\langle\psi|V|\psi\rangle_{100} = {}& (A''\beta - C''\gamma)^2\langle[111]_{\Gamma^{\bar{X}}_{25'}}|V|[111]_{\Gamma^{\bar{X}}_{25'}}\rangle + 2[\beta\gamma(A''^2 - C''^2) + A''C''(\beta^2-\gamma^2)]\langle[111]_{\Gamma^{\bar{X}}_{25'}}|V|[200]_{\Gamma^{\bar{X}}_{25'}}\rangle \\ & + B''^2\langle[111]_{\Gamma^{\bar{x}}_{15}}|V|[111]_{\Gamma^{\bar{x}}_{15}}\rangle\ ,\end{aligned}$$

with

$$\langle[111]_{\Gamma^{\bar{X}}_{25'}}|V|[111]_{\Gamma^{\bar{X}}_{25'}}\rangle = (v_4 - v_{12})(\pi\delta/2)\ ,\quad \langle[111]_{\Gamma^{\bar{X}}_{25'}}|V|[200]_{\Gamma^{\bar{X}}_{25'}}\rangle = (v_3 - v_{11})(\pi\sqrt{2}/4)\delta\ ,$$

$$\langle[111]_{\Gamma^{\bar{x}}_{15}}|V|[111]_{\Gamma^{\bar{x}}_{15}}\rangle = (v_{12} - v_4)(\pi\delta/2)\ .$$

The results are shown in Fig. 3.

---

*On leave from: Laboratoire de Physique Expérimentale, Université Paul Sabatier Toulouse, France.

†NATO Postdoctoral Fellow. Present address: Royal Aircraft Establishment, Farnborough, United Kingdom.

[1] F. Cerdeira, W. Dreybrodt, and M. Cardona, Solid State Commun. 10, 591 (1972).

[2] M. A. Renucci, J. B. Renucci, and M. Cardona, Solid State Commun. 14, 1295 (1974).

[3] M. A. Renucci, J. B. Renucci, R. Zeyher, and M. Cardona, Phys. Rev. B 10, 4309 (1974).

[4] B. A. Weinstein and M. Cardona, Phys. Rev. B 7, 2545 (1973).

[5] G. Nilsson and G. Nelin, Phys. Rev. B 6, 3777 (1972).

[6] B. A. Weinstein and M. Cardona, Solid State Commun. 10, 961 (1972).

[7] P. A. Temple and C. E. Hathaway, Phys. Rev. B 7, 3685 (1973).

[8] R. A. Forman, D. E. Aspnes, and M. Cardona, J. Phys. Chem. Solids 31, 227 (1970).

[9] K. L. Shaklee and R. E. Nahory, Phys. Rev. Lett. 24, 942 (1970).

[10] C. W. Higginbotham (Ph.D. thesis, Brown University, 1970) (unpublished).

[11] E. O. Kane, Phys. Rev. 146, 558 (1966).

[12] F. H. Pollak and G. W. Rubloff, Phys. Rev. Lett. 29, 789 (1972).

[13] P. T. Lin-Chung and K. L. Ngai, Phys. Rev. Lett. 29, 1610 (1972).

[14] K. L. Ngai and E. T. Johnson, Phys. Rev. Lett. 29, 1607 (1972).

[15] B. A. Weinstein and M. Cardona, Phys. Rev. B 8, 2795 (1973).

[16] H. R. Philipp, J. Appl. Phys. 43, 2835 (1972).

[17] R. Loudon, Adv. Phys. 13, 423 (1964).

[18] R. Zeyher (private communication).

[19] I. Goroff and L. Kleinman, Phys. Rev. 132, 1082 (1963).

[20] L. R. Swanson and A. A. Maradudin, Solid State Commun. 8, 859 (1970).

[21] M. I. Bell and R. N. Tyte, Appl. Opt. 13, 1610 (1974).

[22] W. C. Dash and R. Newman, Phys. Rev. 99, 115 (1955).

[23] P. B. Klein, H. Masui, J. J. Song, and R. K. Chang, Solid State Commun. 14, 1163 (1974).

[24] J. S. Kline, M. Cardona, and F. H. Pollak, Helv. Phys. Acta 41, 968 (1968).

[25] C. Gähwiller and F. C. Brown, *Proceedings of the Tenth International Conference on the Physics of Semiconductors, Cambridge, Mass.*, 1970 (US Atomic Energy Commission, 1970), p. 213.

[26] B. A. Weinstein and M. Cardona, Phys. Rev. B 8, 2795 (1973).

[27] R. Schmidt, B. D. McCombe, and M. Cardona, Phys. Rev. B 11, 746 (1975).

[28] K. L. Ngai and A. K. Ganguly, "Proceedings of the NATO Summer Institute," Antwerp, 1973 (unpublished); also K. L. Ngai (private communication).

[29] P. Norton, T. Braggins and H. Levinstein, Phys. Rev. B 8, 5632 (1973).

[30] K. L. Ngai, *Proceedings of the International Conference on the Physics of Semiconductors, Stuttgart, 1974* (B. G. Teubner, Stuttgart, 1974), p. 489.

[31] M. Cardona, in *Atomic Structure and Properties of Solids*, edited by E. Burstein (Academic, New York, 1972), p. 514.

[32] L. Mariot, *Group Theory and Solid State Physics* (Prentice-Hall, Englewood Cliffs, N.J., 1962).

[33] D. Brust, Phys. Rev. 134, A1337 (1964).

[34] M. Cardona and F. Pollak, Phys. Rev. 142, 530 (1966).

[35] E. O. Kane, Phys. Rev. 178, 1368 (1969).